Electrical damage induced by reactive ion-beam etching of lead-zirconate-titanate thin films

Caroline Soyer, Eric Cattan, Denis Remiens

Electrical damage induced by reactive ion-beam etching of lead-zirconate-titanate thin films

Cite as: J. Appl. Phys. **97**, 114110 (2005); https://doi.org/10.1063/1.1923589
Submitted: 10 November 2004 • Accepted: 07 April 2005 • Published Online: 02 June 2005

C. Soyer, E. Cattan and D. Rèmiens

Electrical damage induced by reactive ion-beam etching of lead-zirconate-titanate thin films

C. Soyer,[a] E. Cattan, and D. Rèmiens
Institut d'Electronique de Microélectronique et de Nanotechnologie (IEMN) Unite Mixte de Recherché (UMR) Centre National de la Recherché Scientifique (CNRS) 8520 Departement Opto-Acousto-Electronique (DOAE)/Matériaux et Intégration pour la Microélectronique et les Microsystèmes, Bâtiment P3, Cité Scientifique, 59655 Villeneuve d'Ascq cedex, France

(Received 10 November 2004; accepted 7 April 2005; published online 2 June 2005)

Ion-beam etching of sputtered $Pb(Zr_x,Ti_{1-x})O_3$ (PZT) thin films with x equal to 0.54 grown on $Pt/TiO_x/SiO_2/Si$ substrates has been performed using pure Ar gas and a varying CHF_3/Ar gas mixing ratio. The etch rate dependence on the process parameters (gas composition, current density, and acceleration voltage) has been investigated. PZT etch rate under 40% CHF_3 in Ar can reach 100 nm/min with an acceleration voltage of 900 V and a current density of 0.7 mA/cm^2 (in comparison to 35 nm/min in pure Ar). A selectivity ratio of 8 has been obtained between PZT and photoresist (1.3 in pure Ar). We have evaluated the PZT surface damage by contact mode atomic force microscopy. It appears that the roughness increases less under a gas mixture than under a pure argon beam, and that the preferential etching observed at the grain boundaries under a pure argon beam disappears when we increase the proportion of CHF_3 in the gas mixture. For some etching parameters (current density, acceleration voltage, and gas mixing ratio), we have observed electrical damage. $C(V)$ and hysteresis loops $P(E)$ measurements before and after etching have demonstrated these degradations. We have noted a large decrease of the permittivity after the etching process, independently of the current density and the acceleration voltage. The ferroelectric damage was illustrated by a large increase of the average coercive field after etching in pure argon. The presence of CHF_3 in the plasma partially reduces the damage. © *2005 American Institute of Physics*. [DOI: 10.1063/1.1923589]

I. INTRODUCTION

Ferroelectric thin films have generated a great interest for their applications in memory devices [dynamic random access memory (DRAM) and ferroelectric random access memory (FeRAM)] and in microelectromechanical systems (MEMSs). $Pb(Zr_x,Ti_{1-x})O_3$ (PZT) is one of the most used materials because of their interesting electrical properties, as well ferroelectric as piezoelectric. Patterning of PZT films has become an essential element of device fabrication. Several techniques have been developed for etching: wet chemical etching,[1] ion-beam etching (IBE),[2] reactive ion etching (RIE),[3–5] electron cyclotron resonance (ECR) etching,[6] and inductively coupled plasma (ICP) etching.[7]

The RIE is widely used because it provides, in some etching conditions, high etch rate and selectivity, and also a high degree of anisotropy. But we have chosen to use the reactive ion-beam etching (RIBE) because this technique allows us to separate more easily the two contributions: the sputtering of the elements, and the chemical reactions. Various gas mixtures have been investigated: $Cl_2/C_2F_6/Ar$,[7] Cl_2/Ar,[6] $CF_4/CCl_4/Ar$,[8] and Cl_2/BCl_3.[9]

A majority of the chlorides or fluorides of the metal elements formed during the etching of PZT films are not volatile in the range of pressure and temperature at which we can work. It thus appears that the assistance of an ionic bombardment is necessary to eliminate the compounds formed and present on the surface of the etched material.

The choice of reactive gas is not easy. The vapor pressures of zirconium and titanium chlorides are higher than those of fluorides, which encouraged some teams to use chlorinated gases. However, it is essential to heat the sample if one really wishes to obtain appreciable etch rates. Fluorine plasmas of gases such as CF_4 or C_2F_6 are also currently employed, as well for the etching of silicon as for the etching of the PZT. However, the coexistence of fluorine and hydrogen (for example, CHF_3) is recognized as being favorable to the oxides etching.[10] In addition, the CHF_3 is also a less hazardous gas compared with chlorine containing gases Moreover, contrary to other fluorinated gases, the plasma of fluorinated hydrocarbons does not attack the photoresist quickly. Indeed the etching process is replaced by a polymerization due to the hydrogen presence.[1] Under these conditions, the photoresist can become a very effective etching mask.

The influence of etching parameters on the electrical damage evolution has not been studied sufficiently. It is currently assumed that particles bombardment is primarily responsible for the etching damage whatever the process.[12,13] Both effects, the physical damage and the presence of chemical residual species on the PZT film surface, have not been studied, in particular, through electrical measurements.

In this work, we examine the effect of pure-Ar and CHF_3/Ar (with various ratios) ion-beam etching on the damage created in PZT thin films. Etch rate and selectivity are

[a]Electronic mail: caroline.soyer@univ-valenciennes.fr

investigated in terms of current density, acceleration voltage, and etching gas. The etching of PZT, without an etching mask, has been performed with the aim to observe the evolution of the surface roughness and of the electrical (dielectric and ferroelectric) properties.

II. EXPERIMENTAL PROCEDURE

A. Thin-films growth and etching method

PZT thin films were deposited on $Pt/Ti/SiO_2/Si$ substrates by rf magnetron sputtering with a thickness in the range of 0.9–1.2 μm. Pt and TiO_x layers of 100 and 20 nm, respectively, were deposited on SiO_2/Si substrates by dc sputtering. The PZT sputtering conditions are given elsewhere.[14] The PZT films were annealed at 625 °C for 30 min to form the perovskite phase. All the samples were (110) preferentially oriented, without pyrochlore phase appearance. The average grain size is about 4 μm.

Ion-beam etching of PZT, Pt, and photoresist was investigated by using Veeco Microetch 3 inches. This system was equipped with a Kaufman-type source. It incorporates a filament electron-emitting cathode and an electromagnet mounted at the outside of the ion source chamber. The ion extraction and acceleration system consist of a three-grid assembly. Argon ions were extracted by an acceleration voltage ranging from 0.6 to 1 kV. The current density can be adjusted to its desired value by readjusting the magnetic field, pressure, arc-power, and cathode emission. A filament allows neutralizing the positive charge of the ion beam. The sample holder is water cooled and the temperature is stabilized after an etching time above 5 min. We have taken care to exceed this delay time for each process performed.

To test the possibility of the use of photoresist as an etching mask, several films were coated with conventional photoresist Microposit® S1813 from Shipley) that was patterned by exposure in a mask aligner. After the process the photoresist was removed by acetone, without the need of oxygen plasma or specific remover.

B. Characterization

The etched thickness was determined using Tencor surface profilometer. The surface microstructure of unetched and etched PZT was characterized by atomic force microscopy (AFM). Images in the contact mode AFM were obtained using a Park Scientific Instruments Autoprobe CP.

In order to determine the electrical damage induced by the etching treatment, PZT thin films were etched without a mask. Pt top electrodes were sputtered through a shadow mask on etched PZT for electrical properties measurements. The etched and unetched samples were then compared to evaluate the extent of IBE and RIBE effects. Capacitance and tan δ measurements were performed using an impedance analyzer (HP4192A) at a frequency of 10 kHz and a voltage $V_{ac}=100$ mV. The ferroelectric loops $P(E)$ were measured using a standardized Radiant RT6000 system. The charge option was used; the top electrode was always connected to the drive terminal of the test equipment, while the bottom electrode was connected to the return terminal. Measurements were made before and after a top electrode contact annealing performed at 500 °C. This heating treatment increases the permittivity value (around 10%) in the case of an unetched material. It also allows us to obtain a more symmetrical ferroelectric hysteresis loop, which results from a small increase of the average coercive field.

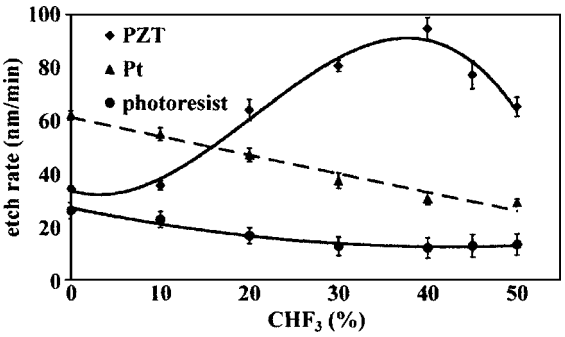

FIG. 1. Etch rate of PZT, Pt, and photoresist according to the percentage of CHF_3 ranging from 0% to 50%. (The curves represent the best fits.)

III. RESULTS AND DISCUSSION

A. Etch rate, selectivity, and surface morphology

By altering the gas mixing ratio CHF_3/Ar in the chamber, a change in the etch rates is observed according to the quantity of fluorinated compounds formed and the efficiency of Ar^+ bombardment. Figure 1 shows the evolution of the etch rate of PZT, platinum, and photoresist for a CHF_3 content ranging from 0% to 50%. Pressure, acceleration voltage, and current density are maintained at 0.026 Pa, 800 V, and 0.7 mA/cm^2, respectively. These two last values were taken in the central part of the acceleration voltage and the current-density ranges which can be covered by the ion source. The PZT etch rate increases quickly beyond 10% of CHF_3 and reaches a maximum close to 95 nm/min for 40% of CHF_3. In comparison, when the etching mechanism is purely physical (pure Ar) the etch rate is of 2.5 times lower than the maximum value reached in the presence of CHF_3. Some authors show similar trends for the etch rate of the PZT thin films, with other reactive gases incorporated with argon. For example, Chung *et al.*[15] observed a maximum PZT etch rate between 40% and 60% of $(Cl_2+C_2F_6)$ added to Ar, as was done by Ting-Ao *et al.*[16] which uses an Ar/SF_6 mixture, and also Baborowski *et al.*[8] with the addition of CF_4 or Cl_4 to argon. In our work, the small amount of CHF_3, between 0% and 10%, is too weak to react sufficiently with the PZT surface. When the content of CHF_3 increases, the etch rate increases. This change results from several processes schemes. The quantity of radicals and reactive ions increases. These species react with the different components of the PZT to form fluorides: $PbF_2, ZrF_4, TiF_4, \ldots$, which are not volatile under our working conditions. The quantity of the compounds formed grows with the concentration of CHF_3 in the gas mixture. However, the bombardment of the Ar^+ ions, and also of the ions obtained by dissociation of the CHF_3, removes these fluorinated compounds by physical sputtering. Moreover, the energy of the incident ions also allows a local activation of the radicals at the surface of the PZT. Consequently, for a proportion of CHF_3 lower than 40%, we are in

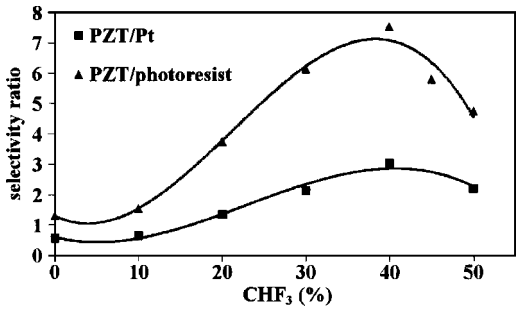

FIG. 2. Dependence of selectivity ratios on the percentage of CHF_3. (The curves represent the best fits.)

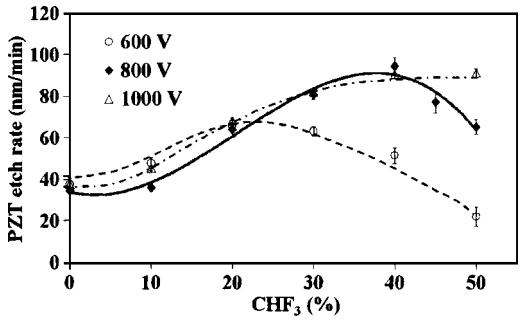

FIG. 3. PZT etch rate according to the CHF_3 content and the acceleration voltage. (The curves represent the best fits.)

a phase where the sputtering rate of the fluorinated compounds is higher than the speed of formation of these same compounds. Beyond 40%, the PZT etch rate decreases. It is an opposite situation: indeed we have simultaneously increased the concentration of reactive species, as well as a reduction of the ionic bombardment effectiveness. The ionic bombardment does not manage any more to eliminate effectively the fluorinated compounds layer.

The etch rate of platinum decreases linearly with the increase of CHF_3 percentage. The progressive reduction of platinum etch rate shows that the CHF_3 is absolutely unsuited to etch this inert material. A strong decrease in the etch rate from 60 to 35 nm/min, proportional to CHF_3 ratio, is observed. The addition of fluorinated or chlorinated gases causes the same reduction of the Pt etch rate.[17,18] Moreover, several studies based on Auger analyses carried out on residues present on the etched surface[17,19] reveal the absence of PtF_x radicals, and show that there is no reaction between the two elements.

The etch rate of the photoresist decreases initially and tends to stabilize from 30% of CHF_3. Loh *et al.*[11] showed that contrary to F_2, CF_4, and SF_6 plasmas, which react with polymers, CHF_3 plasma induces the deposit of a fluorocarbonated film on the surface. In the process of the photoresist etching, the CF_x radicals ($x=0$, 1, or 2) are at the origin of surface polymerization, while the fluorine atoms are the active species for etching.[20] Plasmas of CHF_3 are more rich in CF_2 radicals than the other fluorinated plasmas, hence the domination of a polymerization process. In spite of this supposed photoresist surface polymerization, we did not have difficulties to remove it in acetone.

Figure 2 gives the evolution of PZT to Pt and PZT to photoresist selectivity ratios with increasing CHF_3 concentration. The highest selectivity ratios are obtained for a CHF_3/Ar gas mixing ratio equal to 40/60. As the PZT/photoresist selectivity ratio is between 7 and 8, the photoresist proves to be an effective etching mask. The selectivity between the PZT and platinum is close to 3, and makes of this latter a less useful mask. However, if the thickness of the PZT etched is not too great, it can be possible to use the top electrode as a mask. But, in the case of MEMSs applications, for example, the PZT thickness can be several micrometers. The magnification of selectivity ratios compared to an etching under pure argon is significant: indeed the PZT/photoresist and PZT/Pt selectivities were, respectively, 1.3 and 0.5.

These results of course depend on the ion energy, and thus the acceleration voltage. For example, Fig. 3 shows the evolution of the PZT etch rate with the CHF_3 content and for different acceleration voltage ranging from 600 to 1000 V. At 600 V, we observe that the maximum PZT etch is obtained with a CHF_3 content between 30% and 40%: it reaches 65 nm/min. At 1000 V, a CHF_3 content superior to 50% is necessary to achieve the maximum PZT etch rate. So, during RIBE, the increase of the acceleration is not sufficient to obtain a very high PZT etch rate. The CHF_3 content has to be increased at the same time. Indeed, with increasing CHF_3 concentration, the quantity of fluorinated compounds formed on the surface increases also. At the same time, if the energy of Ar ions increases, they are more efficient to etch these compounds.

Figure 4 shows the AFM images of the PZT surface obtained after etching for various gas mixtures (acceleration voltage and current density are fixed, respectively, to 800 V and 0.7 mA/cm^2). Before etching, the root-mean-square (rms) roughness measured on the surfaces of 20×20 μm^2 ranges between 60 and 80 Å. The average grain size lies between 4 and 5 μm. When the proportion of CHF_3 is about 10%–20%, we have observed that the grain boundaries are preferentially etched (rms=123 Å), as we obtained under pure argon.[21] This behavior is probably the result of two combined phenomena. The first is a difference of the composition between the grain surface and the grain boundary; in particular, a lead excess at the grain boundaries (the lead oxide etch rate is higher than titanium or zirconium oxide etch rates) could explain a deeper etching in these zones. The second is a well-known trenching effect inducing the grain boundaries widening by the ion rebound on the cavity walls formed by two adjacent grains. In both cases it is the physical action of the etching process which dominates. When the content of CHF_3 reaches 40% (rms=140 Å), the grain boundaries are manifested in extra thickness compared to the grain surface, making the effect of preferential etching at the grain boundaries disappear. Figure 5 compares a surface of 15×15 μm^2 for etched (under 40% CHF_3) and unetched PZT films. We clearly observed that the majority of the grain boundaries are etched less quickly than the grains themselves [Fig. 5(b)] and that before etching the grain boundaries do not appear in relief [Fig. 5(a)].

To our knowledge, the team of Baborowski *et al.* observed this characteristic at the grain boundaries of PZT after

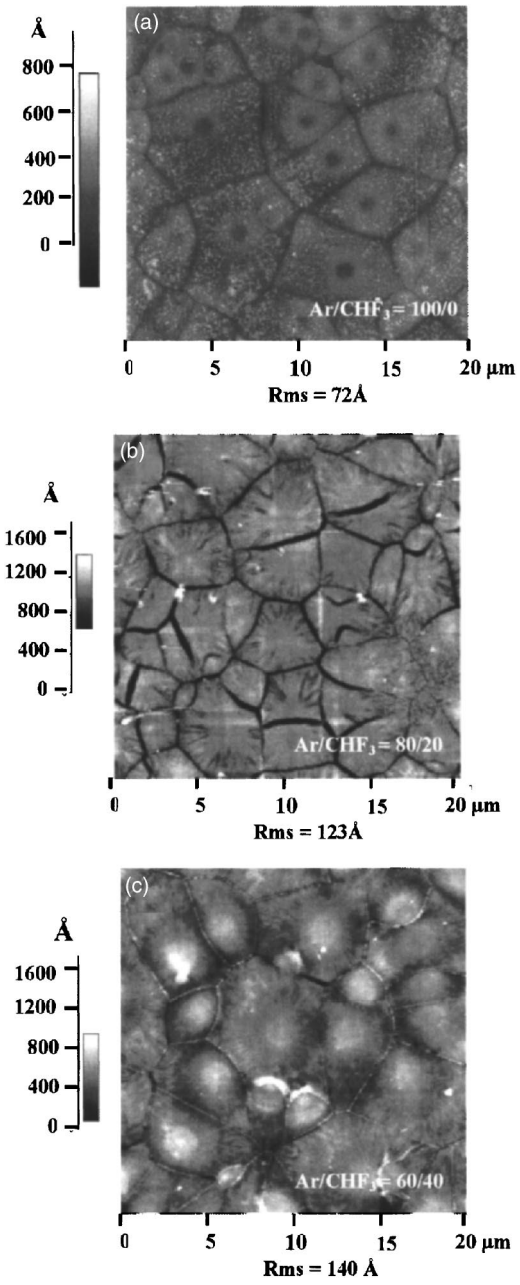

FIG. 4. Observation by AFM of the topography and roughness (rms =root mean square) of PZT films: (a) before etching, (b) etched at $Ar/CHF_3 = 80/20$), and (c) etched at $Ar/CHF_3 = 60/40$.

etching under an ECR-fluorinated plasma.[8] They carried out etchings under CF_4 and noted the appearance of zones in relief, for which the height could range between 170 and 230 nm. They did not observe the same phenomenon under plasma of argon, of Cl_4, nor even under a CF_4/CCl_4 mixture. For our samples, the relief observed in the zones of the grain boundaries is flatter (the height reaches about 10–30 nm, and locally 50 nm). The difference with the results of Baborowski *et al.* can be due to the etching method used. During ion-beam technique, the energy of the ions is greater than during ECR plasma. So, our technique is probably more efficient to etch the relief formed. In our work, the presence of a lead excess at the grain boundaries can explain the topography observed at this location after RIBE. Indeed, when the CHF_3 content increases, the quantity of the lead fluoride formed increases, especially since the lead is in excess.

We note for our samples that the porosities on the grains surface are less marked under CHF_3/Ar mixture than during an etching with pure Ar. We think that these porosities are also related to the preferential sputtering of lead on the grains surface: the formation of PbF_2 prevents the excessive porosities on the surface under CHF_3/Ar mixture. However, the presence of PbF_2 could be damaging for the electrical properties. We did not observe changes of roughness with the acceleration voltage and current density, contrary to the result obtained under pure Ar.[21] Moreover the roughness measured after reactive etching is always lower than the one after pure argon bombardment, whatever the etching parameters are (but it remains higher than the roughness of the unetched PZT film).

Figure 6 shows scanning electron microscopy (SEM) micrographs of etched PZT profile under pure-Ar [Fig. 6(a)] and under $Ar/CHF_3(60/40)$ gas mixture [Fig. 6(b)]. In the two cases, a photoresist mask was used. We observe that the slope of the profile is slightly higher under pure-Ar etching. The profile is over 85°. For the PZT etched by reactive ion-beam etching (RIBE), the profile is over 75°. So, the anisotropy is better after IBE. This result can be explained by the shape of the photoresist mask: the mask does not evolve in the same way during etching with inert or reactive gas. It is important to note the absence of redeposition along the sidewalls of the patterns on SEM micrographs.

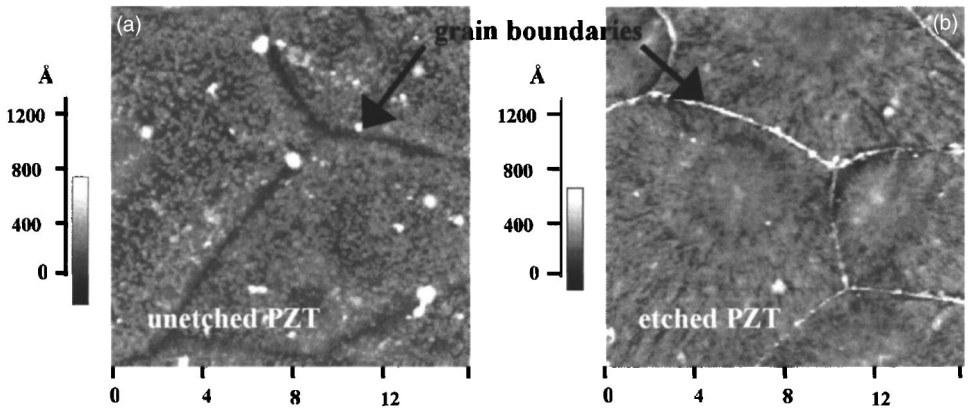

FIG. 5. Comparison of the topography for unetched and etched surfaces ($Ar/CHF_3 = 60/40$).

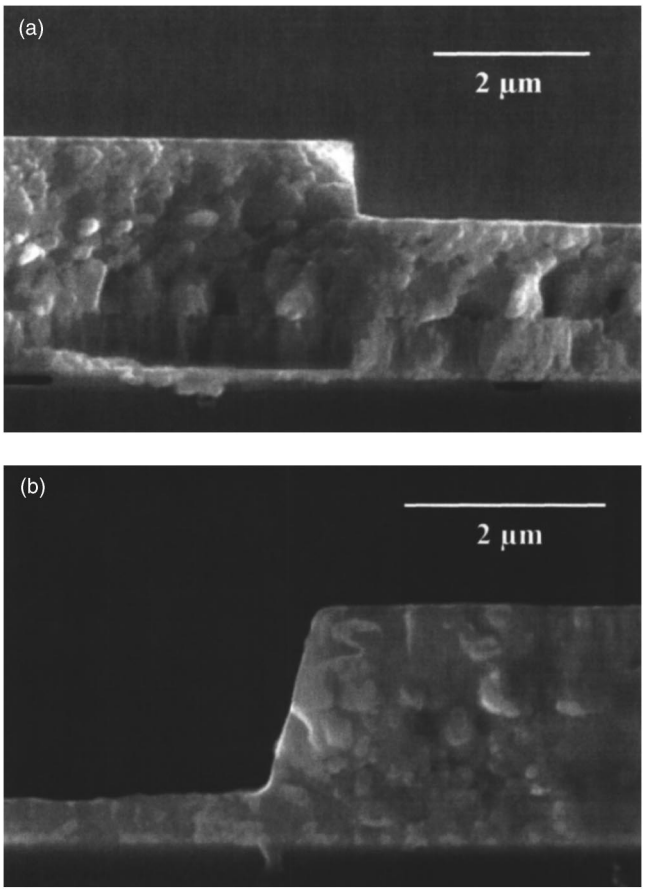

FIG. 6. Observation by SEM of the PZT etching profile obtained: (a) under pure Ar, and (b) under $Ar/CHF_3=60/40$.

B. Electric measurements of etched PZT films

All the electrical results of RIBE films were obtained by using a CHF_3/Ar mixing ratio equal to 40/60 and were compared to the sample etched in pure Ar. The thickness of the films after etching (IBE and RIBE) ranges between 0.5 and 0.6 μm. For greater clarity, our electrical results are presented as the percentage of decrease (−) or percentage of increase (+) relative to the properties of unetched PZT.

Figure 7 shows the evolution of the permittivity with increasing current density. The acceleration voltage is fixed to 800 V. The decrease of permittivity (compared to the unetched film ones) is on the average of 35%–40%. The differences measured between the two ways of etching (IBE and BIBE) are too weak to be significant. We also observed small differences when we changed the acceleration voltage for a fixed current density.

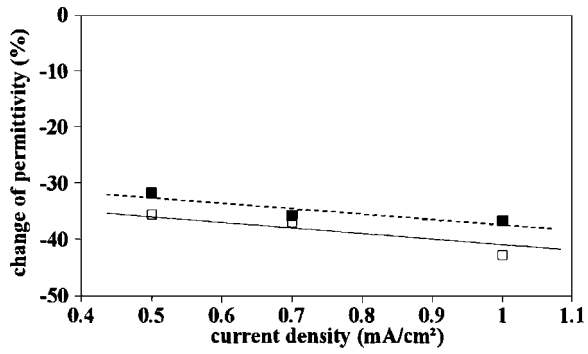

FIG. 7. Evolution of the permittivity according to the current density (acceleration voltage fixed at 800 V), with regard to the permittivity of the unetched film: (□) after IBE, and (■) after RIBE (40% CHF_3). The results were obtained after contact annealing. (The curves represent the best fits.)

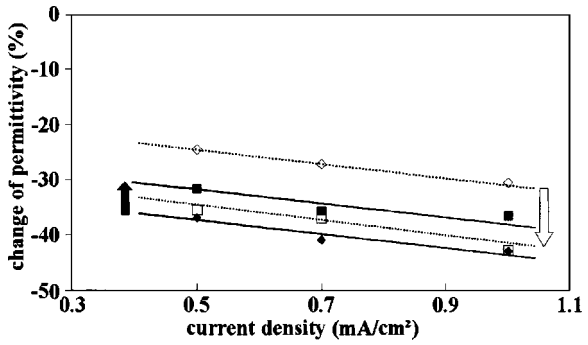

FIG. 8. Evolution of the permittivity with increasing current density (acceleration voltage fixed at 800 V), with regard to the permittivity of the unetched film: (◇) after IBE, before contact annealing; (□) after IBE, after contact annealing, (◆) after RIBE (40% CHF_3), before contact annealing; (■) after RIBE (40% CHF_3), after contact annealing. The arrows represent the change due to contact annealing. (The curves represent the best fits.)

A remarkable point must be noted concerning the role of the contact annealing (Fig. 8). We observe that the degradation of the permittivity, before contact annealing, is larger for PZT etched by RIBE than for PZT etched by IBE: the gap is around 20%. After IBE, the contact annealing increases considerably the fall of the permittivity. This is not the case in reactive etching: on the contrary, the permittivity increases slightly after contact annealing.

Figure 9 visualizes the ferroelectric hysteresis loops obtained before and after etching under Ar and CHF_3/Ar, and after contact annealing. The films are etched under acceleration voltage of 800 V and current density of 0.5 mA/cm^2. The remarkable part of the hysteresis loops after etching under pure argon (and after top electrode annealing) is the large increase of the average coercive field E_a (Fig. 9). E_a is defined as $E_a=(|E_a^+|+|E_a^-|)/2$. Similar loops widening, with various magnitudes, were observed for all etched samples.[21] The coercive field measured after contact annealing can be doubled in some pure Ar etching conditions. During a reactive etching this widening of the loop is largely attenuated while remaining about 60% under any etching parameters.

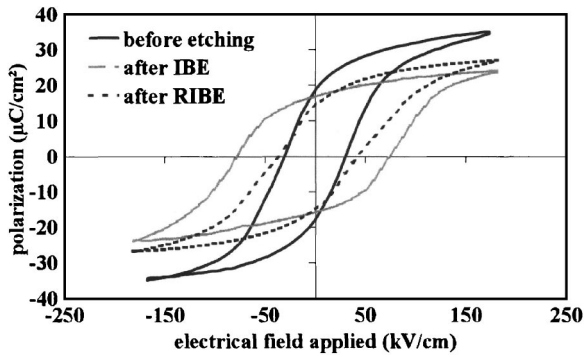

FIG. 9. Comparison of the ferroelectric hysteresis loop obtained before etching, after IBE, and after RIBE (40% CHF_3). (Acceleration voltage =800 V, current density =0.5 mA/cm^2.)

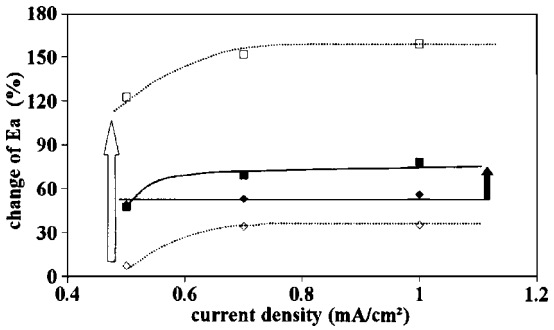

FIG. 10. Evolution of E_a with increasing current density (acceleration fixed at 800 V), with regard to the E_a of the unetched film: (◇) after IBE, before contact annealing; (□) after IBE, after contact annealing; (◆) after RIBE (40% CHF_3), before contact annealing; (■) after RIBE (40% CHF_3), after contact annealing. The arrows represent the change due to contact annealing. (The curves represent the best fits.)

As for the permittivity, the coercive field is more influenced by contact annealing for films etched by IBE than for films etched by RIBE (Fig. 10).

C. Discussion of the damage mechanism

Whereas the microstructural defects are rather different for the ion-beam and reactive ion-beam etching (Fig. 4), the evolution of the permittivity with acceleration voltage and current density follows the same trend (Figs. 7 and 8). While the effects are the same, the causes can differ. In both cases we can think that the presence on the film surface of a layer with a permittivity lower than the one of the bulk film decreases the total permittivity. This surface layer is modified by defects induced by the bombardment. These defects can be of different nature: formation of vacancies by a preferential sputtering of lead, occupation of interstitial sites by argon, the destruction of the structural arrangement of the material, modification of the stress and surface composition, etc. A simple model consists of considering PZT films as being composed of several series capacitors. However, the thickness of this damaged layer is unknown, and it is difficult to assess it: it depends on the existing forces of repulsion between the atoms of the target and the ion beam, of the energy of the atom source, the localization of the impact on the surface, the potential energy of deformation of the lattice, and so on.[22] The roughness of the films surface after etching can be an indication on deterioration zones, supposed having a low permittivity. However, we have shown elsewhere[21] that the roughness is not the associated factor in the modification of the permittivity. Indeed the decrease of the permittivity is not proportional to the increase of the roughness of PZT films etched under pure argon. Moreover, after RIBE, the roughness varies a little (rms=7.5 nm) with the current density and the acceleration voltage parameters, while at the same time the permittivity is strongly affected as shown on Fig. 7. In addition, we observe here that in spite of an important difference in the roughness of the surface after IBE and RIBE (Fig. 4), the decrease of the permittivity is similar. While having changed the gas ratio, we change the nature of the generated defects. When the proportion of argon decreases by 40%, the quantity of crystalline defects in the surface layer is the smallest. On the other hand, it is very possible that the fluorinated compounds are present on the surface of the PZT. This layer can constitute a nonferroelectric film, of unknown thickness. For example, Lee *et al.*[23] showed that after having etched 50 nm of PZT by an inductive coupling plasma (ICP) technique using a $Ar–Cl_2–C_2F_6$ gas mixture, they had formed a layer of 10 nm thick containing fluorine compounds, and not having the perovskite structure. During IBE, we can consider that the defects formed are "physical," while during RIBE they are "physical and chemical." The thickness and the electrical properties of the damaged layer present at the surface are unknown, but differ certainly with the etching technique used. We have observed that the degradation of the permittivity is similar in both cases (IBE and RIBE). We can conclude that the presence of a damaged layer is not the only parameter to take into account. Another mechanism of degradation has to be considered to explain the results observed.

A reduction in the mobility of the domains and domain walls is also a possible explanation for the permittivity decrease. After etching, the various defects (electric or elastic), born from the interaction of the atoms with the surface of the film, are distributed randomly. The free charges injected are attracted in the areas of polarization discontinuity, in particular, in the domains walls. If the charges are trapped, they then make obstruction to the walls motion. In addition, the grain boundaries preferentially etched under pure Ar let suppose that they form favorable zones to the accumulation of defects. Indeed, a reduction in the maximum polarization and an increase in the average coercive field generally give evidence to a clamping of the domain-wall motion.

When the films are etched under CHF_3/Ar, the grain boundaries are not preferentially etched; on the contrary they appear in extra- thickness. So, the nature of the defects located at the grain boundaries is probably different according to the etching technique used. As a consequence, the mechanism of domain-wall pinning and the influence of a thin layer (with a low permittivity) located at the surface are not the same after IBE or RIBE.

In addition, the effect of the contact annealing on the permittivity brings another information. We think that the strong permittivity decrease of the films etched under Ar, observed after the contact annealing, results from a migration of the surface defects towards the bulk of the film. On one hand, this increases the depth on which the layer is damaged. On the other hand, the defects, initially distributed randomly, can migrate towards the domain walls to reduce their mobility more. On the contrary, the contact annealing of a film etched under reactive gas improves the permittivity of the film as we usually observe it for an unetched film. We thus think that the etching with a CHF_3/Ar mixture does not generate mobile defects that are able to increase the pinning of the domain-wall motion. In this case the fall of the permittivity is explained mainly by the formation of a surface layer with a low permittivity.

These results are corroborated by the evolution of the coercive field observed in Fig. 10. Indeed the strong increase in the average coercive field after contact annealing for films etched under pure argon is well explained by a strong pin-

ning of the domain-wall motion. This phenomenon is much weaker in the case of a film etched under CHF_3/Ar (Figs. 9 and 10) where we limit the phenomenon of the domain-wall clamping.

Remnant polarization is only slightly reduced (around 3%) in pure argon etching (Fig. 9), while during RIBE a decrease of 10% can be observed. This is explained by the following reason: initially, before applying an external field, the defects (linked to the lattice distortion, to the presence of gap or atoms in interstitial sites, etc.) present in the material are distributed at random. Progressively with the application of the field, these defects move in a favorable direction from a point of view of low energy, in relation with the orientation of spontaneous polarization or with the existing stress. Maximum polarization is then reached. Once these defects are aligned, it becomes very difficult to change the polarization orientation or to move the domain walls. The switch of the domains when the electric field decreases is incomplete, which induces a relatively high remnant polarization, compared to the maximum polarization. It is said that the domain walls are clamped by the defects.[24] The defects, responsible for domain pinning, are less numerous in reactive etching. So, domain switching is freer.

The evolution of the maximum polarization is not presented, but the trend is similar to the permittivity one. In particular, the effect of IBE and RIBE is of the same order whatever the parameters of etching. The effects of contact annealing observed on the permittivity remain valid for maximum polarization.

However, the effect of domain-wall pinning is not the single one to take into account. Indeed, we have also observed that the permittivity and maximum polarization are degraded after RIBE overall as much than under pure argon etch. If only the domain mobility were involved in the mechanism of degradation, we should have measured better dielectric properties and polarizations after RIBE. So, the presence of a nonferroelectric layer on the surface of the PZT causes obviously a decrease of the permittivity and moreover tilts the ferroelectric loop.[25] The tilt of the hysteresis loop results in a reduction of coercive field and polarizations, all the more marked since the thickness of the nonferroelectric layer increases.

In conclusion, during RIBE, two different ways of degradation are in competition. On one hand, the presence of a surface layer containing particularly fluorine compounds seems to be the major factor responsible for the permittivity and remnant polarization decrease. On the other hand, the increase of the average coercive field is mainly due to the loss of the domain-wall mobility.

IV. CONCLUSION

In this study, we have shown the differences in the mechanisms of degradations induced by IBE and RIBE. In a first part, we have demonstrated that RIBE with an Ar/CHF_3 gas mixture is suitable to improve the PZT etch rate and the selectivity ratio. The photoresist appears to be an effective etching mask. We have established that the surface roughness increases after etching: this increase is larger after IBE. The topographical defects are different: after IBE, we observe a preferential etching at the grain boundaries whereas after RIBE, we observe an extra thickness at this location.

We have also demonstrated that this degradation of the PZT surface is not directly responsible for the electrical damages. Two other phenomena can explain the electrical results: the formation of a surface layer having poor properties, and a domain-wall pinning phenomenon. The addition of CHF_3 modifies the nature of the defects induced, particularly by the formation of fluorine compounds. Moreover, the influence of the ionic bombardment is also reduced after RIBE.

It is thus difficult to clearly identify the degradation processes. We have actually various phenomena in competition. It seems that the effect related to the presence on the surface of a layer containing fluorine is dominating when it concerns the evolution of the permittivity or average remnant polarization. Conversely, it is the loss of mobility of the domain walls which seems to dictate the coercive field.

[1] S. Mancha, Ferroelectrics **135**, 131 (1992).
[2] T. Kawagughi, H. Adachi, K. Setsune, O. Yamazaki, and K. Wasa, Appl. Opt. **23**, 2187 (1984).
[3] K. Saito, J. H. Choi, T. Fukuda, and M. Ohue, Jpn. J. Appl. Phys., Part 2 **31**, L1260 (1992).
[4] D. P. Vijay, S. B. Desu, and W. Pan, J. Electrochem. Soc. **140**, 2635 (1993).
[5] W. Pan, S. B. Desu, In K. Yoo, and D. P. Vijay, J. Mater. Res. **9**, 2976 (1994).
[6] S. Yokoyama, Y. Ito, K. Ishihara, K. Hamada, T. Ohnishi, J. Kudo, and K. Sakiyama, Jpn. J. Appl. Phys., Part 1 **34**, 767 (1995).
[7] C. W. Chung and C. J. Kim, Jpn. J. Appl. Phys., Part 1 **36**, 2747 (1997).
[8] J. Baborowski, P. Muralt, N. Ledermann, E. Colla, A. Seifert, S. Gentil, and N. Setter, Integr. Ferroelectr. **31**, 261 (2001).
[9] N. Ikegami, T. Matsui, and J. Kanamori, Jpn. J. Appl. Phys., Part 1 **35**, 2505 (1996).
[10] K. Shima, N. Mitsugi, and H. Nagata, J. Mater. Res. **13**, 527 (1998).
[11] I. H. Loh, M. Klausner, R. F. Baddour, and R. E. Cohen, Polym. Eng. Sci. **27**, 861 (1987).
[12] J. J. Van Glabbeek, G. A. C. M. Spierings, M. J. E. Ulenaers, G. J. M. Mans, and P. K. Larsen, Mater. Res. Soc. Symp. Proc. **310**, 127 (1993).
[13] G. Suchaneck, R. Tews, and G. Gerlach, Surf. Coat. Technol. **116–119**, 456 (1999).
[14] G. Velu, D. Rèmiens, and B. Thierry, J. Eur. Ceram. Soc. **17**, 1749 (1997).
[15] C. W. Chung, W. I. Lee, and J. K. Lee, Integr. Ferroelectr. **11**, 259 (1995).
[16] T. Ting-Ao, C. Zheng, L. Ning, and Z. Si-Xun, Ferroelectrics **232**, 47 (1999).
[17] W. J. Yoo, J. H. Hahm, H. W. Kim, C. O. Jung, Y. B. Koh, and M. Y. Lee, Jpn. J. Appl. Phys., Part 1 **35**, 2501 (1996).
[18] J. Baborowski, P. Muralt, N. Ledermann, and S. Hiboux, Vacuum **56**, 51 (2000).
[19] E. Farrell, K. R. Milkove, C. Wang, and D. E. Kotecki, Integr. Ferroelectr. **16**, 109 (1997).
[20] R. D'Agostino, F. Cramarossa, and S. de Benedictis, Plasma Chem. Plasma Process. **2**, 213 (1982).
[21] C. Soyer, E. Cattan, and D. Rèmiens, J. Appl. Phys. **92**, 1048 (2002).
[22] K. J. Boyd, D. Marton, J. W. Rabalais, S. Uhlmann, and T. Frauenheim, J. Vac. Sci. Technol. A **16**, 444 (1998).
[23] S. H. Lee, H. J. Joo, J. P. Kim, J. H. Jung, M. K. Ryu, S. S. Lee, and M. S. Jang, J. Korean Phys. Soc. **35**, 1172 (1999).
[24] D. Damjanovic, Rep. Prog. Phys. **61**, 1267 (1998).
[25] A. K. Tagantsev, M. Landivar, E. Colla, and N. Setter, J. Appl. Phys. **78**, 2623 (1995).